1   **Numerical Analysis of the Primary Processes Controlling Oxygen**

2   **Dynamics on the Louisiana Shelf**

Liuqian Yu[1], Katja Fennel[1], Arnaud Laurent[1], Michael C. Murrell[2] and John C. Lehrter[2]

[1]Department of Oceanography, Dalhousie University, Halifax, Nova Scotia, Canada

3   [2]US Environmental Protection Agency, Gulf Ecology Division, 1 Sabine Island Dr., Gulf

4   Breeze, FL 32561, USA

5

6   **Abstract**

7   The Louisiana shelf in the northern Gulf of Mexico receives large amounts of freshwater

8   and nutrients from the Mississippi/Atchafalaya River system. These river inputs

9   contribute to widespread bottom-water hypoxia every summer. In this study, we use a

10 physical-biogeochemical model that explicitly simulates oxygen sources and sinks on the

11 Louisiana shelf to identify the key mechanisms controlling hypoxia development. First,

12 we validate the model simulation against observed dissolved oxygen concentrations,

13 primary production, water column respiration, and sediment oxygen consumption. In the

14 model simulation, heterotrophy is prevalent in shelf waters throughout the year except

15 near the mouths of the Mississippi and Atchafalaya Rivers where primary production

16 exceeds respiratory oxygen consumption during June and July. During this time, efflux

17 of oxygen to the atmosphere, driven by photosynthesis and surface warming, becomes a

18 significant oxygen sink. A substantial fraction of primary production occurs below the

19 pycnocline in summer. We investigate whether this primary production below the

20 pycnocline is mitigating the development of hypoxic conditions with the help of a

21 sensitivity experiment where we disable biological processes in the water column (i.e.

22 primary production and water column respiration). With this experiment we show that

23 below-pycnocline primary production reduces the spatial extent of hypoxic bottom waters

24 only slightly. Our results suggest that the combination of physical processes (advection

25 and vertical diffusion) and sediment oxygen consumption largely determine the spatial

26 extent and dynamics of hypoxia on the Louisiana shelf.

1. Introduction

The Louisiana shelf (LA shelf) in the northern Gulf of Mexico receives large inputs of freshwater, nutrients and organic matter from the Mississippi/Atchafalaya River system and experiences widespread hypoxia (oxygen concentrations < 2 mg l^{-1} or 62.5 mmol m^{-3}) in bottom waters every summer (Rabalais et al. 2007; Bianchi et al. 2010). The classic paradigm for explaining the recurring hypoxic conditions on the LA shelf is that high nutrient inputs from the river stimulate high rates of primary production in coastal waters; as this organic matter sinks below the pycnocline and is respired, dissolved oxygen (DO) becomes depleted due to a combination of high microbial respiration and low re-oxygenation of the bottom waters because of strong stratification (Rabalais et al. 2002).

While the statistical linkage between spring nutrient loads and the spatial extent of the summer hypoxic area is well documented (Turner et al., 2005; Greene et al., 2009; Forrest et al., 2011), the distribution of hypoxia on the LA shelf is known to be the integrated result of various physical and biogeochemical processes that interact non-linearly (Bianchi et al. 2010; Fennel et al. 2011). Rowe and Chapman (2002) suggested that as the distance from the river mouth increases, the primary driver of hypoxia changes from deposition of riverine organic matter to biological production and respiration and finally to physical stratification. Model simulations (Bierman et al., 1994; Breed et al., 2004; Eldridge and Roelke 2010) also show that the dominant processes contributing to hypoxia change in westward direction, namely allochthonous organic matter accounts for most of DO consumption near the Mississippi river mouth and autochthounous organic matter dominates DO consumption farther west. Hetland and DiMarco (2008) suggested that the differences in vertical stratification within the Mississippi and Atchafalaya River

50   plumes lead to differences in the dominant type of respiration responsible for hypoxia

51   with water column respiration driving hypoxia near the Mississippi River plume and

52   benthic respiration controlling hypoxia near Atchafalaya Bay and further west. Recent

53   work suggests that the main axis of variability in hydrography and metabolism is inshore

54   to offshore on the shelf (Lehrter et al. 2012; Murrell et al., 2013a; Lehrter et al., 2013;

55   Fry et al., 2014).

56   Understanding the occurrence of hypoxia on the LA shelf requires quantitative

57   knowledge of the mechanisms controlling DO dynamics. Generally, the distribution of

58   DO is determined by physical processes (air-sea flux, horizontal advection, vertical

59   mixing across the pycnocline) and biogeochemical processes (photosynthetic production,

60   respiration in the water column and sediments, and oxidation of reduced substances)

61   (Testa and Kemp, 2011). The magnitudes and spatial and temporal dynamics of these

62   processes on the LA shelf are as of now poorly constrained.

63   Circulation over the LA shelf displays two distinct modes (Cochrane and Kelly, 1986;

64   Cho et al., 1998): an upcoast circulation mode during the dominantly upwelling-favorable

65   (westerly) winds in summer (June to August) versus westward flow during the

66   dominantly downwelling-favorable (easterly) winds for the rest of the year. Previous

67   statistical studies (Forrest et al., 2011; Feng et al., 2012) have shown that the observed

68   hypoxic extent is correlated to the duration of upwelling-favorable wind. Feng et al.

69   (2014) further showed that the wind influences the distribution of low salinity, high

70   chlorophyll water on the shelf and thereby the bottom water DO concentrations and

71   hypoxic area.

72   A substantial fraction of phytoplankton production is observed below the pycnocline

73   (Lehrter et al., 2009) and even at the sediment-water interface when light is available

74   (Lehrter et al., 2014), but the effect of sub-pycnocline production on bottom water

75   hypoxia is not well known. Eldridge and Morse (2008) highlighted the importance of

76   benthic respiration as a DO sink at the beginning and end of hypoxic events, and

77   suggested water column respiration in bottom water near the pycnocline as primary O_2

78   sink once hypoxia has developed. Quinones-Rivera et al. (2007, 2010) estimated benthic

79   respiration to account for ~73% of the total DO loss within 1 m of the bottom sediments

80   during summer based on $\delta^{18}O$ measurements and an isotope fractionation model,

81   whereas Murrell and Lehrter (2011) found that benthic respiration only contributes on

82   average 20$\pm$4% of total respiration below the pycnocline. The relative contributions of

83   benthic and water column respiration are strongly affected by the assumed depth of the

84   bottom layer.

85   In order to better understand the relative importance of these processes, considerable

86   efforts have been invested in modeling the DO dynamics and hypoxia within the system.

87   These models range from relatively simple regression models (Turner et al., 2005, 2006;

88   Greene et al., 2009; Forrest et al., 2011; Feng et al. 2012) to more complex process

89   simulations that emphasize either biogeochemical processes in simplified physical

90   frameworks (Justić et al. 1996, 2002; Eldridge and Morse, 2008; Green et al. 2008) or

91   physical circulation using detailed hydrographic models with simple parameterizations of

92   biogeochemical process (Hetland and DiMarco 2008; Lehrter et al., 2013). More recently

93   a number of fully coupled physical-biogeochemical models have become available

94   (Fennel et al. 2013; Laurent and Fennel 2014; Feng et al. 2014; Justić and Wang 2014).

95   Coupled models of DO dynamics and circulation have been used successfully in other

96   coastal systems with seasonal hypoxia including Chesapeake Bay (i.e., Cerco and Cole,

97   1993; Cerco, 1995). More recently, Li et al. (2015) coupled an empirical DO model

98   derived from observations with a high-resolution hydrodynamic model to derive a DO

99   budget for Chesapeake Bay. An even simpler empirical DO parameterization was used by

100   Scully (2013) to illustrate the important role of physical forcing in the formation of

101   seasonal hypoxia. Both, Li et al. (2015) and Scully (2013) obtained a realistic simulation

102   of the seasonal cycle of DO and spatial distributions of hypoxic water.

103   Here we use a coupled physical-biogeochemical model for the LA shelf described in

104   Fennel et al. (2011, 2013) that was recently extended to include phosphate by Laurent et

105   al. (2012) and Laurent and Fennel (2014). The biogeochemical model explicitly simulates

106   DO and is coupled to the realistic 3-dimensional circulation model of Hetland and

107   DiMarco (Hetland and DiMarco 2008, Hetland et al. 2012). Here we build upon the

108   earlier work to identify the key processes controlling DO dynamics.

109   The manuscript is organized as follows. First we describe the coupled physical-

110   biogeochemical model and its DO source and sink terms. Then we validate model-

111   simulated DO and oxygen production and consumption rates against available

112   observations. We explore spatial and temporal patterns of water column metabolism

113   across the shelf and its interaction with air-sea fluxes. We also analyze the summer DO

114   balance for different regions which allows us to identify the key controlling processes and

115   how they vary in space. Finally, we examine the role that sub-pycnocline primary

116   production plays in hypoxia generation.

117

2. Model description

118   **2. Model description**

119   Our physical model is the Regional Ocean Modelling System (Haidvogel et al. 2008,

120   ROMS, http://myroms.org) configured for the Mississippi/Atchafalaya outflow region as

121   described in Hetland and DiMarco (2008, 2012). The model grid covers the Louisiana

122   continental shelf with a horizontal resolution ranging from ~20 km in the southwestern

123   corner to 1 km near the Mississippi Delta, and has 20 terrain-following vertical layers

124   with increased resolution near the surface and bottom (Fig. 1). The model uses a fourth-

125   order horizontal advection scheme for tracers and a third-order upwind scheme for the

126   advection term in the momentum equation. Vertical gradients are calculated with

127   conservative parabolic splines, and vertical mixing is parameterized using the Mellor and

128   Yamada (1982) turbulent closure scheme. An average profile of temperature and salinity,

129   based on historical hydrographic data (Boyer et al., 2006) and assumed to be horizontally

130   uniform, is used as physical boundary condition. At the three open boundaries, gradient

131   conditions are used for the free surface, radiation conditions for the three-dimensional

132   velocities, and a Flather (1976) condition with no mean barotropic background flow for

133   the two-dimensional velocities. The model is forced with 3-hourly winds from the NCEP

134   North American Regional Reanalysis (NARR) and climatological surface heat and

135   freshwater fluxes from da Silva et al. (1994a, b). Freshwater inputs from the Mississippi

136   and Atchafalaya rivers are based on daily measurements of transport by the US Army

137   Corps of Engineers at Tarbert Landing and Simmesport, respectively.

138   The biological component of the model uses the nitrogen cycle model of Fennel et al.

139   (2011, 2013) but was extended to include phosphate (Laurent et al., 2012) and river

140   dissolved organic matter as additional state variables. The model is a relatively simple

141 representation of the pelagic nitrogen (N) cycle, including two species of dissolved

142 inorganic N, nitrate (NO_3) and ammonium (NH_4), phosphorus (PO_4), one phytoplankton

143 group (Phy), chlorophyll (Chl) as a separate state variable to allow for photoacclimation,

144 one zooplankton group (Zoo), two pools of detritus representing large, fast-sinking

145 particles (LDet), and suspended, small particles (SDet), and river-born dissolved organic

146 matter (RDOM). Combined with the freshwater discharge described above, the model

147 receives river nutrients (NO_3 and NH_4) and organic matter based on the US Geological

148 Survey (USGS) estimates (http://toxics.usgs.gov/). More specifically, river dissolved

149 organic nitrogen (DON) was determined as the difference between filtered Total Kjeldahl

150 Nitrogen (TKN) and NH_4; and particulate organic nitrogen (PON) was defined as the

151 difference between unfiltered and filtered TKN (Fig. 2). Different from our previously

152 published simulations where river organic nitrogen enters the pool of SDet in the model

153 without distinguishing between dissolved and particulate fractions, here river DON and

154 PON enter the pools of RDOM and SDet, respectively. The only biological term in the

155 equation for RDOM is remineralization to NH_4 in the water column. We chose a

156 remineralization rate of 0.03 d^{-1} for RDOM, an order of magnitude lower than that of

157 small detritus (0.3 d^{-1}) to reflect the observation that riverine dissolved organic matter is

158 less labile than phytoplankton-derived organic matter (Shen et al., 2012). A schematic of

159 the extended N cycle model is shown in Figure 3. Also shown are the biological sources

160 and sinks of DO, including photosynthetic production, nitrification, respiration in water

161 column and sediment, and the air-sea flux of oxygen across the air-sea interface. At the

162 open boundaries NO_3, PO_4 and oxygen were prescribed using the NODC World Ocean

163 Atlas. All other biological state variables at the boundary were set to small positive

164 values. Model parameterization and previous validations were described in Fennel et al.

165 (2006, 2011, 2013), Laurent et al. (2012), Laurent and Fennel (2014). For completeness'

166 sake, all parameter values are given in Table S1 of the Online Supplement.

167   The equation for the *DO* conservation is given by

168 $$\frac{\partial DO}{\partial t} = -\left(u\frac{\partial DO}{\partial x} + v\frac{\partial DO}{\partial y} + w\frac{\partial DO}{\partial z}\right) + \frac{\partial}{\partial z}\left(K_v\frac{\partial DO}{\partial z}\right) + PP + WR + F_{bf} \tag{1}$$

169 where *x* and *y* represent the two horizontal coordinates and *z* the vertical coordinate, *u*, *v*,

170 and *w* (m s^{-1}) represent velocity components in *x*-, *y*-, and *z*-coordinates, respectively, and

171 K_v is the vertical diffusivity (m s^{-2}). On the right-hand side of the Eq. (1), the first term

172 represents horizontal and vertical advection of DO, and the second term is the vertical

173 diffusion of DO (horizontal diffusivity K_H is set 0 in the model and hence we neglected

174 horizontal diffusion terms in equation 1). Here the advection and diffusion terms are

175 computed using the advanced numerical schemes build into the ROMS hydrodynamic

176 model. The term PP is the primary production and WR represents the sum of water

177 column respiration and nitrification. Although not strictly accurate, the use of the

178 terminology WR is consistent with the use of WR in the observational literature where

179 measurements of water column oxygen consumption include the contribution of

180 nitrification. The term F_{bf} represents the boundary oxygen fluxes, namely the air-sea flux

181 of oxygen at the top layer and the sediment oxygen consumption at the bottom layer, the

182 parameterizations of which are detailed below.

183   Following Fennel et al. (2013), an air-sea flux of oxygen ($F_{air-sea}$, in units of mmol

184 O$_2$ m^{-2} d^{-1}) is prescribed in the top layer of the model as:

185 $$F_{air-sea} = \frac{vk_{O2}}{\Delta z}(DO_{sat} - DO), \tag{2}$$

186   where DO and DO_{sat} are the oxygen concentration and concentration at saturation,

187   respectively, Δz is the thickness of the respective grid box, and vk_{O2} is the gas exchange

188   coefficient for oxygen based on Wanninkhof (1992), such that:

189     $vk_{O2} = 0.31\, u_{10}^2 \sqrt{\dfrac{660}{Sc_{Ox}}},$ (3)

190   where u_{10} is the wind speed at 10 m above the sea surface, and Sc_{Ox} is the Schmidt

191   number, calculated as in Wanninkhof (1992).

192   The parameterization for Sediment Oxygen Consumption (SOC) used in this study was

193   developed by Hetland and DiMarco (2008) and based on observed sediment oxygen

194   fluxes from Rowe et al. (2002). In this parameterization, SOC (mmol O_2 m^{-2} d^{-1}) linearly

195   increases with increasing bottom water oxygen (DO, mmol O_2 m^{-3}) for concentrations

196   lower than 50 mmol O_2 m^{-3} and saturates when concentrations are higher than 100 mmol

197   O_2 m^{-3}. Also, SOC is dependent on temperature (T, °C) such that it doubles for every 10°C

198   temperature increase (i.e., $Q_{10} = 2$). The equation is given as follows:

199     $SOC = 6\,[mmol\; O_2\; m^{-2}d^{-1}] * 2^{T/10°C} * \left(1 - \exp\left(-\dfrac{DO}{30[mmol\; O_2\; m^{-3}]}\right)\right).$ (4)

200   In Fennel et al. (2013) this parameterization was extended to include an NH$_4$ flux into

201   the bottom water proportional to oxygen uptake by the sediments. Therefore, organic

202   matter sinking out of the water column essentially leaves the system while empirically

203   determined fluxes of oxygen into the sediments and ammonium out of the sediments are

204   prescribed.

205   Motivated by the model-data comparisons, described below, we conducted a sensitivity

206   experiment where a spatially and temporally constant oxygen consumption rate (1.5

207   mmol O_2 m^{-3} d^{-1}) was added to the water column oxygen pool (simulation denoted as

208   'Model+CCR'). In order to distinguish between the role of biological processes in the

209   water column (primary production and water column respiration, denoted as PP and WR,

210   respectively) and the combination of physical transport and sediment respiration, we

211   conducted two further sensitivity experiments where all biological processes in the water

212   column were turned off (denoted as 'Model w/o PP and WR' and 'Model+CCR w/o PP

213   and WR' in comparison to the full model simulation and Model+CCR, respectively).

214   All simulations were run from 1 January 2004 to 31 December 2007. For model

215   analysis we defined four geographical zones across the Louisiana continental shelf: three

216   sub-regions associated with the Mississippi River plume (Mississippi Delta, Mississippi

217   Intermediate, Mid-shelf), and another sub-region associated with the Atchafalaya River

218   plume (Atchafalaya Plume) (Fig. 1). These four sub-regions cover most stations that

219   comprise the observational data sets used for model validation: (1) DO concentrations

220   from Rabalais et al. (2007), Nunally et al. (2013), Murrell et al. (2013b), and the

221   Mechanisms Controlling Hypoxia (MCH) program; (2) in situ measurements of water

222   column respiration rates from 10 cruises during spring, summer and fall from 2003 to

223   2007 (Murrell et al., 2013a); (3) the concurrent measurements of phytoplankton

224   production from Lehrter et al. (2009); (4) benthic flux measurements from Rowe et al.

225   (2002), Murrell and Lehrter (2011), Lehrter et al. (2012), and McCarthy et al. (2013).

226   Locations for the observed primary production and water column respiration rates are

227   shown as black dots in Figure 1.

228

229   **3. Results**

3.1 Simulated oxygen dynamics and model validation

Time series of simulated and observed bottom DO both show a seasonal cycle reaching a maximum between December and February and minimum between July and August (Fig. 4). In summer the median of simulated bottom DO is consistently larger than observations in the Mississippi Intermediate region, but otherwise observations and simulation agree well. Simulated bottom DO falls within the observed range of variability for all 4 regions.

We report model bias and root mean square error (RMSE) as statistical measures of agreement between simulated and observed bottom DO in Table 1. Bias was calculated as model minus observations; thus a positive bias indicates that the model overestimates the observations. Table 1 indicates that the model overestimates the observed bottom DO in all regions with an average bias of 33.7 mmol O_2 m^{-3}. Based on this comparison, the model performs best in the Mid-shelf region (bias of 15.6 mmol O_2 m^{-3}) and worst in the Mississippi Delta region (bias of 43.3 mmol O_2 m^{-3}).

Profiles of bias between simulated and observed DO profiles are shown in Figure 5 for the summer months. Simulated DO often overestimates observed DO, but remains typically within one standard deviation of the observations except for the bottom layer (e.g. in June).

Observed and simulated rates of primary production (PP) and water column respiration (WR) are shown in Figure 6, and statistical measures of model-data agreement are given in Table 2. The model simulates the observed PP reasonably well, but underestimates the WR observations, although the model is within one standard deviation of the observations (Fig. 6 and Table 2).

253   Simulated SOC within all 4 regions is plotted against bottom DO and compared with

254   available observations in Figure 7. Simulated SOC increases with increasing bottom DO

255   for oxygen concentrations below ~80 mmol O_2 m^{-3} and declines thereafter because of the

256   temperature effect (SOC halves for each temperature decrease of 10 ℃). SOC

257   observations from different sources vary over a large range from 0 to 40 mmol O_2 m^{-2} d^{-1}

258   (Fig. 7). Simulated SOC is at the upper range of the available observations. Model bias in

259   Table 3 indicates that the median of simulated SOC overestimates the observed SOC

260   when combining all sources (average bias 18.2 mmol O_2 m^{-2} d^{-1}).

261   **3.2 Validation of the Model+CCR simulation**

262   The model biases described in previous section (i.e. the underestimation of WR and

263   overestimation of SOC) motivated us to carry out an additional simulation (Model+CCR)

264   with increased WR. The additional, constant oxygen consumption rate (1.5 mmol O_2 m^{-3}

265   d^{-1}) was determined from Table 2 (average bias of 30.8 mmol O_2 m^{-2} d^{-1} divided by the

266   average water column depth of 20.4 m) and should compensate for the bias in model-

267   simulated WR.

268   Compared with the previous model simulation, Model+CCR reduces the overall model

269   data discrepancy in WR (average bias of -1.0 mmol O_2 m^{-2} d^{-1}) but overestimates the

270   observed WR in the Mid-shelf region (bias of 35.6 mmol O_2 m^{-2} d^{-1}) (Fig. 6 and Table 2).

271   The increased WR draws down the simulated DO concentrations, improving agreement

272   between the observed and simulated bottom DO in all regions (average bias of 9.1 mmol

273   O_2 m^{-3}) except in the Mid-shelf region where the observed bottom DO is significantly

274   underestimated (bias of -18.8 mmol O_2 m^{-3}) (Fig. 4 and Table 1). Compared to the

275   previous simulation, the reduced DO concentrations throughout the water column in

276 Model+CCR generally improve the model performance with lower biases, except for the

277 Mid-shelf region in June and July (Fig. 5). The reduced bottom DO concentrations in

278 Model+CCR also lead to a reduction in the simulated SOC (as SOC is dependent on

279 bottom DO) and thereby slightly improve the agreement between simulated and observed

280 SOC with lower RMSE and bias (average bias of 14.9 mmol O_2 m^{-2} d^{-1}) (Fig. 7 and Table

281 3).

282 **3.3 Oxygen balance**

283 In this section, we evaluate the DO balance for the summer period (June to August) for

284 different regions of the LA shelf to identify the key processes controlling hypoxia. We

285 focus the detailed analysis on the model simulation without additional WR; results from

286 Model+CCR will be discussed at the end of the section. For simplicity, we are

287 considering that oxygen consumption due to nitrification to be included in the respiration

288 term, and not as a separate process for deriving the oxygen balance. Though we are

289 referring to the sum of respiration and nitrification as WR, we recognize that nitrification

290 is a chemoautotrophic process. While not strictly accurate, this is consistent with the use

291 of WR in the observational literature where measurements of water column oxygen

292 consumption include the contribution of nitrification.

293 We first explore the simulated seasonal and spatial patterns in water column

294 metabolism across the shelf and its interaction with the air-sea flux of oxygen (Fig. 8).

295 The Mississippi Delta and Atchafalaya Plume regions, which are directly impacted by the

296 river, transit from autotrophy in June and July to heterotrophy for the rest of the year. The

297 Mississippi Intermediate and Mid-shelf regions, however, are heterotrophic throughout

298 the year. In terms of air-sea exchange, oxygen is outgassing during summer and taken up

299 during the rest of the year in all sub-regions, corresponding to the seasonal pattern in

300 water column metabolism (more heterotrophic in winter and less heterotrophic or

301 autotrophic in summer) and the seasonal cycle of surface water temperatures, which

302 affect oxygen solubility contributing to outgassing in summer and uptake in winter. The

303 oxygen flux into the ocean increases with the degree of heterotrophy, demonstrating the

304 important role of air-sea gas exchange in replenishing DO in the water column.

305 When considering an oxygen balance for the water column it is useful to distinguish

306 distinct vertical layers. We considered the following three layers in our analysis of the

307 summer oxygen balance: a surface layer above the main pycnocline, a mid-layer

308 extending from the main pycnocline to 5 m above the sediment and a 5-m thick bottom

309 layer above the sediment (i.e., the layer where hypoxia occurs most frequently, as

310 demonstrated in Figure 6 in Fennel et al., 2013). We defined the pycnocline as the depth

311 of maximum Brunt-Vaisala Frequency (Pond and Pickard, 1983) and restricted our

312 analysis to horizontal grid cells where all three layers existed (i.e. a main pycnocline was

313 present and was more than 5 m above the bottom). We then integrated the terms in Eq. (1)

314 vertically over each layer at each desired grid cell on each desired day. The advection and

315 diffusion terms were evaluated as divergences, namely fluxes of DO into or out of the

316 given volume through advection or diffusion. Finally we averaged the integrated results

317 over all grid cells within a selected sub-region and over June to August in order to obtain

318 the summer oxygen balance for the sub-regions.

319 Figure 9 shows the summer oxygen balance in the three layers and four sub-regions

320 (numbers are provided in Table S2 of the Online Supplement). The surface layers in all

321 four sub-regions are autotrophic while the bottom layers are heterotrophic (Fig. 9). In the

322 surface layer, biochemical processes (PP and WR) far exceed physical transport of

323 oxygen. The positive net community production and decreasing oxygen solubility

324 associated with the increasing water temperature in summer lead to oxygen outgassing to

325 the atmosphere and net transport of oxygen downward to deeper waters.

326   The mid-layer is autotrophic in all four sub-regions as well, with an average PP of 48%

327 occurring below the pycnocline and 38% in the mid-layer. About 10% of PP occurs

328 within the 5-m bottom layer where hypoxia occurs most frequently (Fig. 9). We

329 compared the simulation results with observations from Lehrter et al. (2009), as

330 percentage of production below the pycnocline for each cruise (Table 4). Considering the

331 rather large observed standard deviations, the percentages of sub-pycnocline PP in the

332 simulations (18.6 - 40.9%) agree well with observations (23.3 - 38.7%).

333   On average the sub-pycnocline PP offsets 68% of total respiration below the pycnocline

334 and 27% of total respiration within the 5-m bottom layer (Fig. 9). The percentages are

335 higher in 2006 (a drought year) where PP offsets 72% of total respiration below

336 pycnocline and 31% of total respiration within the bottom 5 m.

337   The 5-m bottom layer is heterotrophic in all sub-regions with SOC representing the

338 single largest oxygen flux (Fig. 9).   The SOC accounts for 36% of total respiratory

339 oxygen demand below the pycnocline when averaged over the shelf and summer months.

340 The fraction of SOC rises to 68% when limited to the bottom 5 m (Fig. 9). Driven by the

341 strong vertical DO gradient in the water column, vertical diffusion is the primary mode of

342 DO replenishment for the bottom layer offsetting on average 32% of total respiration over

343 the shelf. Advection, driven by the typical summer upwelling circulation on the LA shelf,

344 is another important DO source for bottom waters offsetting on average 29% of total

345 respiration shelf-wide.

346   Adding WR in the Model+CCR simulation impacted the summer oxygen balance by

347 making the water column more heterotrophic and decreasing the relative contributions of

348 SOC and WR to total respiration (Table S3 and Fig. S3). In Model+CCR the mid layers

349 in all sub-regions and all three layers in Mid-shelf region become heterotrophic in

350 summer months. Also, the simulated fraction of SOC to total respiration averaged over

351 the 4 sub-regions during summer decreases from 36% to 26% within below-pycnocline

352 water layer and from 68% to 57% within the bottom 5-m layer.

353 **3.4 Role of sub-pycnocline PP in hypoxia generation**

354   Time series of simulated hypoxic area from the sensitivity run without biological

355 processes in the water column (Model w/o PP and WR) are shown in comparison to the

356 full model and the observed hypoxic extent in Figure 10. The temporal evolution of

357 hypoxic area is almost identical in both simulations, with 'Model w/o PP and WR'

358 simulating an only slightly larger hypoxic area in summer. A similar pattern is observed

359 for simulated hypoxic volume (Fig. S1) and for the simulations with the additional

360 oxygen sink (Fig. S4).

361

362 **4. Discussion**

363 **4.1 Simulated oxygen dynamics and model validation**

364   Overall, the model simulates the evolution of oxygen and the magnitudes and spatial

365 distribution of PP well, but tends to overestimate bottom DO and underestimate WR

366   (within one standard deviation of observations). One possible explanation is that the

367   model does not receive any dissolved or particulate organic matter inputs from estuarine

368   sources other than the Mississippi and Atchafalaya rivers. Several recent studies (Bianchi

369   et al. 2010, Murrell et al. 2013a, and Fry et al. 2014) suggested that the inshore coastal

370   waters represent a source of oxygen-consuming organic matter that may be episodically

371   transported onto the LA shelf.

372   The model also overestimates the observed SOC from all sources, especially those

373   observed by Lehrter et al. (2012) and Murrell and Lehrter (2011) (Fig. 7, Table 3). Using

374   the same model as in this study, Fennel et al. (2013) have shown that generation of

375   hypoxia on the LA shelf is very sensitive to the parameterization of SOC, primarily

376   because the hypoxic conditions on the shelf are restricted to a relatively thin layer above

377   the sediment. Fennel et al. (2013) have further shown that the SOC parameterization

378   based on observations from Rowe et al. (2002), which is used in this study, performed

379   best in simulating the observed hypoxic extent whereas parameterization based on lower

380   SOC values from Murrell and Lehrter (2011) led to almost no hypoxia in this model. The

381   apparent discrepancy between SOC observations and parameterizations used in

382   mechanistic models remains to be reconciled. One explanation could be that empirical

383   SOC measurements underestimate the true oxygen demand, because they do not account

384   for accumulation of reduced metabolites of anaerobic metabolism (e.g., NH_4^+, HS^-, Fe^{2+}).

385   Accumulation of anaerobic metabolites can be episodically important in scavenging

386   oxygen, thus acting to maintain hypoxic conditions during periods when traditional SOC

387   measurements suggest a small DO sink. This interpretation is supported by Lehrter et al.

388   (2012) who found that DIC fluxes (a better measure of total oxygen demand) were

389 relatively constant and insensitive to overlying DO concentration. Another explanation

390 could be that the thickness of the simulated bottom boundary layer is overestimated. If

391 this is the case, SOC would have to be larger than in reality in order to produce hypoxic

392 bottom water. Future work on validating the expression and dynamics of the bottom

393 boundary layer and its effect on hypoxia dynamics will address this question.

394 The SOC parameterization has the inherent limitation that it does not account for spatial

395 variability in the supply of particulate organic matter reaching the sediment. An

396 alternative model, where SOC varies responsive to the amount of organic matter sinking

397 to the sediment (Fennel et al. 2011, 2013), essentially simulated identical results as

398 presented here. While the SOC parameterization used here is simple, it does include two

399 key parameters known to modulate SOC: temperature and dissolved oxygen.

400 In order to assess the effects of the model biases in WR we conducted a sensitivity

401 experiment where an additional, constant oxygen consumption rate was applied to the

402 water column DO based on observed WR rates from Murrell et al. (2013a). This

403 generally improves the comparisons among measured and simulated WR, bottom water

404 DO and SOC except in the Mid-shelf region where WR is overestimated and bottom DO

405 is underestimated. The increased WR and slightly decreased SOC in the Model+CCR

406 simulation also reduce the SOC fraction of total respiratory oxygen demand.

407 **4.2. Primary processes controlling oxygen dynamics**

408 The simulated seasonal transition from autotrophy to heterotrophy in the Mississippi

409 Delta and Atchafalaya Plume regions has previously been reported in mesohaline waters

410 (salinity: 15-29) in the Mississippi River plume (Breed et al., 2004). The Mississippi

411 Intermediate and Mid-shelf regions were heterotrophic throughout the year, implying a

412 net import of organic carbon. This result is consistent with the observations of Murrell et

413 al. (2013a) who found net heterotrophy on the western shelf and in deeper waters of the

414 LA shelf. A more recent study by Fry et al. (2014) also suggested that the autotrophic

415 near-river and nearshore areas could be net source regions of carbon fueling hypoxia in

416 adjacent mid-shelf waters.

417 Despite the heterotrophy, the main sink for oxygen is outgassing in the Mississippi

418 Intermediate and Mid-shelf regions during the summer hypoxic season. This result is

419 consistent with frequent observations of supersaturated DO concentrations in surface

420 plume waters, particularly in the Louisiana Bight region (Murrell et al. 2013b). The

421 simultaneous occurrence of heterotrophy and outgassing of oxygen is primarily due to

422 density stratification of the water column, which isolates the autotrophic upper waters

423 that actively exchange oxygen with the atmosphere from the heterotrophic waters below.

424 As shown in the summer DO balance (Fig. 9), the surface layers above the pycnocline

425 were autotrophic in all sub-regions, driving outgassing of oxygen to the atmosphere

426 despite the whole water column being heterotrophic. The decreased oxygen solubility of

427 warmer waters typical of summer conditions also promotes outgassing, but the effect is

428 relatively small compared to the autotrophy in surface waters (oxygen gas-exchange is

429 fast and the summer change in water temperature is relatively small on the LA shelf). We

430 have carried out sensitivity experiments where we doubled and halved the air-sea gas

431 exchange coefficient (results not presented in the manuscript) and found that the model

432 results are insensitive to the air-sea gas exchange rates, likely because the air-sea oxygen

433 flux is fast.

434   It has previously been demonstrated, based on observations, that a strong near-surface

435   pycnocline is a prerequisite for hypoxia on the LA shelf, while a weaker, near-bottom

436   pycnocline determines the hypoxic layer that actually forms (Wiseman et al., 1997). This

437   was confirmed by model simulations (Fennel et al., 2013), which show that hypoxia is

438   constrained to a thin layer above the sediment over large parts of the shelf. A more recent

439   retrospective analysis of data collected during shelf-wide sampling cruises reported that

440   the 27-year (1985-2011) average thickness of the bottom hypoxic layer is 3.9 m and that

441   there was an increasing trend in hypoxic layer thickness from 1985 to 2011 (Obenour et

442   al., 2013).

443   Consistent with observations by Lehrter et al. (2009), our model demonstrated that a

444   large fraction of PP occurred below the pycnocline and even within bottom 5-m water

445   (Fig. 9, Table 4). This is presumably because the euphotic zone extends well below the

446   pycnocline and sometimes to the bottom on the LA shelf (Chen et al., 2000; Lehrter et al.,

447   2009). Lehrter et al. (2009) also observed that the euphotic zone in non-plume areas

448   (salinity>31) is deeper than in plume areas, and that the average shelf-wide light

449   attenuation strongly correlates with freshwater discharge from the Mississippi and

450   Atchafalaya rivers. In agreement with these observations, the simulated percentage of

451   sub-pycnocline PP is higher in the Mississippi Intermediate region (52% below the

452   pycnocline and 13.6% in the 5-m bottom layer) than in the Delta region (48% and 8.3%,

453   respectively), and higher throughout the shelf in 2006 (a drought year with low

454   freshwater discharge) than in average over the 4 years simulated (52% compared to 48%).

455   The importance of physical transport in replenishing bottom-water DO pools has been

456   found in other coastal systems with seasonal hypoxia including Chesapeake Bay, where

457 Kemp et al. (1992) estimated that in summer the vertical oxygen flux across the

458 pycnocline and the net longitudinal oxygen exchange offset ~55% and ~38% of total

459 respiration below the pycnocline, respectively. More recent modeling work by Li et al.

460 (2015) estimated that vertical diffusion and net advective fluxes respectively offset ~27%

461 and ~64% of total respiration in the bottom 10 m during summer. Kemp et al. (1992) also

462 showed that increased biological consumption of DO in bottom waters of Chesapeake

463 Bay increases horizontal and vertical DO gradients and thereby increases physical

464 transport of DO to the bottom waters during March to July. On the LA shelf the

465 occasional occurrence of tropical storms and hurricanes can rapidly erode stratification

466 and replenish bottom waters with DO. The lateral advection of oxygenated water from

467 adjacent deep basins during upwelling-favorable wind conditions can also increase

468 bottom-water DO on the LA shelf (Rabalais et al, 2007).

469 The result that SOC is the dominant oxygen sink in waters directly overlying the

470 sediments (within 5 m above the bottom) is consistent with previous observational

471 estimates for the LA shelf. Quinones-Rivera et al. (2007) estimated that SOC accounts for

472 ~73% of the total DO loss within 1 m of the sediments during summer based on $\delta^{18}O$

473 measurements and an isotope fractionation model. Since the isotope approach only

474 provides relative fractions of sediment and water column respiration, we cannot directly

475 compare SOC and WR from Quinones-Rivera et al. (2007) to our simulations. However,

476 the simulated proportions of sediment respiration to total respiration (on average 36%

477 below pycnocline and 68% in the 5-m bottom layer) are consistent with the estimates of

478 Quinones-Rivera et al. (2007). Adding the additional DO sink decreased the proportions

479 of SOC to total respiration (26% below the pycnocline and 57% in the 5-m bottom layer)

480   but did not change the model result that SOC is the dominant DO sink in the bottom 5 m,

481   demonstrating the relative sensitivity of the model to the SOC parameterization used.

482   **4.3 Role of sub-pycnocline PP in hypoxia generation**

483   The summer oxygen balance presented in the previous section suggests that physical

484   transport processes and sediment respiration are major drivers of oxygen dynamics on the

485   LA shelf, and that PP below the pycnocline may mitigate hypoxic conditions. However,

486   in a sensitivity experiment where we disabled all biological processes in the water

487   column the spatial extent of hypoxic bottom waters is only slightly reduced, suggesting

488   that PP below the pycnocline has only a minor effect on hypoxia.

489

490   **5. Summary and conclusions**

491   In this study we used a physical-biogeochemical model to investigate the dynamics of

492   dissolved oxygen and hypoxia on the LA shelf and to identify the key controlling

493   processes. Comparisons with observations demonstrate that the model simulates the

494   evolution of oxygen well but tends to overestimate bottom DO and SOC, and

495   underestimates WR. When adding a constant oxygen consumption rate in the water

496   column to correct the bias in WR rates, the model-simulated oxygen dynamics agree

497   better with observations in all sub-regions except the Mid-shelf. This result suggests that

498   organic matter from inshore waters may need to be included in future versions of the

499   model.

500   Consistent with observations of Murrell et al. (2013a), our model demonstrated that the

501   LA shelf is essentially heterotrophic throughout the year except for the areas directly

502 impacted by rivers during June and July. This implies a net import of organic carbon on

503 the LA shelf. Air-sea gas exchange was the primary mode of replenishing the very

504 heterotrophic waters in non-summer months with relatively strong mixing. However, in

505 summer, stratification isolates the autotrophic surface from the heterotrophic lower

506 waters. In the Mississippi Intermediate and Mid-shelf regions this isolation results in

507 significant outgassing of oxygen across the air-sea interface despite a heterotrophic water

508 column, exacerbating the risk of hypoxia in these regions.

509   In summer, the model indicates that a substantial fraction of primary production

510 (~48%) occurs below the pycnocline and about 10% of primary production occurs within

511 5 m of the bottom where hypoxia forms most frequently. In a sensitivity experiment

512 where biological processes in the water column (i.e. PP and WR) were turned off we

513 demonstrate that the below-pycnocline PP mitigates hypoxia only slightly, and that

514 physical processes and sediment oxygen consumption together largely determine the

515 spatial extent and dynamics of hypoxia on the LA shelf.

516

520

521 **References**

522 Bianchi, T.S., DiMarco, S.F., Cowan Jr, J.H., Hetland, R.D., Chapman, P., Day, J.W., and

523   Allison, M.A.: The science of hypoxia in the Northern Gulf of Mexico: A review,

524   Sci. Total Environ., 408, 1471-1484, 2010.

525   Bierman, V.J., Hinz, S.C., Zhu, D.W., Wiseman, W.J. Jr, Rabalais, N.N., and Turner, R.E.:

526   Preliminary mass balance model of primary productivity and dissolved oxygen in the

527   Mississippi River plume/inner gulf shelf region, Estuar., 17, 886-899, 1994.

528   Boyer, T. P., Antonov, J.I., Garcia, H.E., Johnson, D.R., Locarnini, R.A., Mishonov, A.V.,

529   Pitcher, M.T., Baranova, O.K., and Smolyar, I.V.: World Ocean Database 2005,

530   edited by: Levitus, S., NOAA Atlas NESDIS 60, US Government Printing Office,

531   Washington, DC, 190 pp., DVDs, 2006.

532   Breed, G.A., Jackson, G.A., and Richardson T.L.: Sedimentation, carbon export and food

533   web structure in the Mississippi River plume described by inverse analysis, Mar.

534   Ecol. Prog. Ser., 278, 35-51, 2004.

535   Cerco, C.F.: Response of Chesapeake Bay to nutrient load reductions, J. Environ. Eng.,

536   121(8), 549-557, 1995.

537   Cerco, C.F. and Cole, T.M.: Three-dimensional eutrophication model of Chesapeake Bay,

538   J. Environ. Eng., 119(6), 1006-1025, 1993.

539   Chen, X., Lohrenz, S.E., and Wiesenburg, D.A.: Distribution and controlling mechanisms

540   of primary production on the Louisiana-Texas continental shelf, J. Mar. Syst., 25,

541   179-207, 2000.

542   Cho, K., Reid, R.O., and Nowlin, W.D.: Objectively mapped stream function fields on the

543   Texas–Louisiana shelf based on 32 months of moored current meter data, J. Geophys.

544   Res., 103 (C5), 10377-10390, 1998.

545   Cochrane, J.D. and Kelly, F.J.: Low-frequency circulation on the Texas-Louisiana

546   continental shelf, J. Geophys. Res., 91 (C9), 10645-10659, 1986.

547   da Silva, A.M., Young-Molling, C.C., and Levitus, S.: Atlas of Surface Marine Data 1994

548   Vol. 3, Anomalies of fluxes of heat and momentum. NOAA Atlas NESDIS 8, Natl.

549   Oceanic and Atmos. Admin., Silver Spring, MD, 1994a.

550   da Silva, A.M., Young-Molling, C.C., and Levitus, S.: Atlas of Surface Marine Data 1994

551   Vol. 4, Anomalies of fresh water fluxes, NOAA Atlas NESDIS 9, Natl. Oceanic and

552   Atmos. Admin., Silver Spring, MD, 1994b.

553   Eldridge, P.M. and Morse, J.W.: Origins and temporal scales of hypoxia on the Louisiana

554   shelf: Importance of benthic and sub-pycnocline water metabolism. Mar. Chem.,

555   108, 159-171, 2008.

556   Eldridge, P.M. and Roelke, D.L.: Origins and scales of hypoxia on the Louisiana shelf:

557   importance of seasonal plankton dynamics and river nutrients and discharge. Ecol.

558   Model., 221, 1028-1042, 2010.

559   Feng, Y., DiMarco, S.F., and Jackson, G.A.: Relative role of wind forcing and riverine

560   nutrient input on the extent of hypoxia in the northern Gulf of Mexico, Geophys.

561   Res. Lett., 39, L09601, doi:10.1029/2012GL051192, 2012.

562   Feng, Y., Fennel, K., Jackson, G.A., DiMarco, S.F., and Hetland, R.D.: A model study of

563   the response of hypoxia to upwelling-favorable wind on the northern Gulf of Mexico

564   shelf, J. Mar. Syst., 131, 63-73, 2014.

565   Fennel, K., Wilkin, J., Levin, J., Moisan, J., O'Reilly, J., and Haidvogel, D.: Nitrogen

566   cycling in the Middle Atlantic Bight: results from a three-dimensional model and

567   implications for the North Atlantic nitrogen budget, Global Biogeochem. Cy., 20,

568   GB3007, doi:10.1029/2005GB002456, 2006.

569   Fennel, K., Hetland, R.D., Feng, Y., and DiMarco, S.: A coupled physical-biological

570   model of the Norththern Gulf of Mexico shelf: model description, validation and

571   analysis of phytoplankton variability, Biogeosciences, 8, 1881-1899, 2011.

572   Fennel, K., Hu, J., Laurent, A., Marta-Almeida, M., and Hetland, R.D.: Sensitivity of

573   hypoxia predictions for the Northern Gulf of Mexico to sediment oxygen

574   consumption and model nesting, J. Geophys. Res., 118, 990-1002, 2013.

575   Flather, R. A.: A tidal model of the northwest European continental shelf, Memoires de la

576   Societe Royale de Sciences de Liege, 141-164, 1976.

577   Forrest, D., Hetland, R.D., and DiMarco, S.: Multivariable statistical regression models

578   of the areal extent of hypoxia over the Texas-Louisiana continental shelf. Environ.

579   Res. Lett., 6, 1-10, 2011.

580   Fry, B., Justic´, D., Riekenberg, P., Swenson, E., Turner, R.E., Wang, L., Pride, L.,

581   Rabalais, N.N., Kurtz, J.C., Lehrter, J.C., Murrell, M.C., Shadwick, E.H. and Boyd,

582   B.: Carbon dynamics on the Louisiana continental shelf and cross-shelf feeding of

583   hypoxia. Estuar. Coast., DOI 10.1007/s12237-014-9863-9, 2014

584   Green, R.E., Breed, G.A., Dagg, M.J., and Lohrenz, S.E.: Modeling the response of

585   primary production and sedimentation to variable nitrate loading in the Mississippi

586   River plume, Cont. Shelf Res., 28, 1451-1465, 2008.

587   Greene, R.M., Lehrter, J., and Hagy, J.: Multiple regression models for hindcasting and

588   forecasting midsummer hypoxia in the Gulf of Mexico, Ecol. Appl., 19, 1161-1175,

589   2009.

590   Haidvogel, D. B., Arango, H., Budgell,W. P., Cornuelle, B. D., Curchitser, E., Di

591   Lorenzo, E., Fennel, K., Geyer, W. R., Hermann, A. J., Lanerolle, L., Levin, J.,

592   McWilliams, J. C., Miller, A. J., Moore, A. M., Powell, T. M., Shchepetkin, A. F.,

593   Sherwood, C. R., Signell, R. P., Warner, J. C., and Wilkin, J.: Ocean forecasting in

594   terrain-following coordinates: formulation and skill assessment of the regional ocean

595   modeling system, J. Comput. Phys., 227, 3595-3624, 2008.

596   Hetland, R.D. and DiMarco, S.F.: How does the character of oxygen demand control the

597   structure of hypoxia on the Texas-Louisiana continental shelf?, J. Mar. Syst., 70, 49-

598   62, 2008.

599   Hetland, R.D. and DiMarco, S.F.: Skill assessment of a hydrodynamic model of

600   circulation over the Texas- Louisiana continental shelf, Ocean Modell., 43/44, 64-76,

601   2012.

602   Justić, D., Rabalais, N.N., and Turner, R.E.: Effects of climate change on hypoxia in

603   coastal waters: a doubled CO_2 scenario for the northern Gulf of Mexico. Limnol.

604   Oceanogr., 41, 992-1003, 1996.

605   Justić, D., Rabalais, N.N., and Turner, R.E.: Modeling the impacts of decadal changes in

606   riverine nutrient fluxes on coastal eutrophication near the Mississippi River delta,

607   Ecol. Model., 152, 33-46, 2002.

608   Justić, D. and Wang, L.: Assessing temporal and spatial variability of hypoxia over the

609   inner Louisiana–upper Texas shelf: Application of an unstructured-grid three-

610   dimensional coupled hydrodynamic-water quality model, Cont. Shelf Res., 72, 163-

611   179, 2014.

612   Kemp, W.M., Sampou, P.A., Garber, J., Tuttle, J., and Boynton, W.R.: Seasonal

613   depletion of oxygen from bottom waters of Chesapeake Bay: Roles of benthic and

614   planktonic respiration and physical exchange processes, Mar. Ecol.-Prog. Ser., 85,

615   137-152, 1992.

616 Laurent, A., Fennel, K., Hu, J., and Hetland, R.D.: Simulating the effects of phosphorus

617   limitation in the Mississippi and Atchafalaya River plumes, Biogeosciences, 9, 4707-

618   4723, 2012.

619 Laurent, A. and Fennel, K.: Simulated reduction of hypoxia in the northern Gulf of

620   Mexico due to phosphorus limitation, Elementa, doi:10.12952/journal.elementa.

621   000022, 2014.

622 Lehrter, J.C., Murrell, M.C., and Kurtz, J.C.: Interactions between Mississippi River

623   inputs, light, and phytoplankton biomass and phytoplankton production on the

624   Louisiana continental shelf, Cont. Shelf Res., 29, 1861-1872, 2009.

625 Lehrter, J.C., Beddick, D.L., Devereux, R., Yates, D.F., and Murrell, M.C.: Sediment-

626   water fluxes of dissolved inorganic carbon, O_2, nutrients, and N_2 from the hypoxic

627   region of the Louisiana continental shelf, Biogeochemistry, 109, 233-252, 2012.

628 Lehrter, J.C., Ko, D.S., Murrell, M.C., Hagy, J.D., Schaeffer, B.A., Greene, R.M., Gould,

629   R.W., and Penta, B.: Nutrient distributions, transports, and budgets on the inner

630   margin of a river-dominated continental shelf, J. Geophys. Res.- Oceans, 118, 4822-

631   4838, 2013.

632 Lehrter, J.C., Fry, B., and Murrell, M.C.: Microphytobenthos production potential and

633   contribution to bottom layer oxygen dynamics on the inner Louisiana continential

634   shelf, Bull. Mar. Sci., 90(3): 765-780, 2014.

635 Li, Y., Li, M., and Kemp, M.: A budget analysis of bottom-water dissolved oxygen in

636   Chesapeake Bay, Estuar. Coast, DOI 10.1007/s12237-014-9928-9, 2015.

637 McCarthy, M.J., Carini, S.A., Liu, Z., Ostrom, N.E., and Gardner, W.S.: Oxygen

638   consumption in the water column and sediments of the northern Gulf of Mexico

639   hypoxic zone., Estuar. Coast. Shelf. Sci., 123, 46-53, 2013.

640 Mellor, G.L. and Yamada, T.: Development of a turbulence closure model for geophysical

641   fluid problems. Rev. Geophys. Space Phys., 20, 851-875, 1982.

642 Murrell, M.C. and Lehrter, J.C.: Sediment and lower water column oxygen consumption

643   in the seasonally hypoxic region of the Louisiana continental shelf, Estuar. Coasts,

644   34, 912-924, 2011.

645 Murrell, M.C., Stanley, R.S., and Lehrter, J.C.: Plankton community respiration, net

646   ecosystem metabolism, and oxygen dynamics on the Louisana continental shelf:

647   implications for hypoxia, Cont. Shelf Res., 52, 27-38, 2013a.

648 Murrell, M.C., Beddick, D.L., Devereux, R., Greene, R.M., Hagy, J.D., Jarvis, B.M.,

649   Kurtz, J.C., Lehrter, J.C. and Yates, D.F. (2013) Gulf of Mexico hypoxia research

650   program data report: 2002-2007, p. 217, U. S. Environmental Protection Agency,

651   Washington, DC, EPA/600/R-13/257, http://tinyurl.com/ko9wj7j, 2013b

652 Nunnally, C.C., Rowe, G.T., Thornton, D.C.O., and Quigg, A.: Sediment oxygen

653   consumption and nutrient regeneration in the Northern Gulf of Mexico Hypoxic

654   Zone, J. Coast. Res., 63, 84-96, 2013.

655 Obenour, D.R., Scavia, D., Rabalais, N.N., Turner, R.E., and Michalak, A.M.:

656   Retrospective analysis of midsummer hypoxic area and volume in the Northern Gulf

657   of Mexico, 1985–2011, Environ. Sci. Technol., 47, 9808-9815, 2013.

658 Pond, S. and Pickard, G.L.: Introductory dynamical oceanography, 2nd edition Pergamon

659   Press, Oxford. 1983.

660 Quinones-Rivera, Z.J., Wissel, B., Justic, D., and Fry, B.: Partitioning oxygen sources

661   and sinks in a stratified, eutrophic coastal ecosystem using stable oxygen isotopes,

662   Mar. Ecol. Prog. Ser., 342, 69-83, 2007.

663   Quinones-Rivera, Z.J., Wissel, B., Rabalais, N.N, and Justic, D.: Effects of biological and

664   physical factors on seasonal oxygen dynamics in a stratified, eutrophic coastal

665   ecosystem, Limnol. Oceanogr., 55 (1), 289-304, 2010.

666   Rabalais, N.N., Turner, R.E., and Wiseman, W.J.: Gulf of Mexico hypoxia, a.k.a. "The

667   Dead Zone", Ann. Rev. Ecol. Syst., 33, 235-263, 2002.

668   Rabalais, N.N., Turner, R.E., Sen Gupta, B.K., Boesch, D.F., Chapman, P., and Murrell,

669   M.C.: Hypoxia in the northern Gulf of Mexico: Does the science support the plan to

670   reduce, mitigate, and control hypoxia?, Estuar. Coast., 30, 753-772, 2007.

671   Rowe, G.T. and Chapman, P.: Continental shelf hypoxia: some nagging questions, Gulf

672   of Mexico Sci., 20, 153-160, 2002.

673   Rowe, G.T., Kaeki, M.E.C., Morse, J.W., Boland, G.S., and Briones, E.G.E.: Sediment

674   community metabolism associated with continental shelf hypoxia, northern Gulf of

675   Mexico, Estuar., 25 (6), 1097-1106, 2002.

676   Scully, M. E.: Physical controls on hypoxia in Chesapeake Bay: A numerical modeling

677   study, J. Geophys. Res., 118, 1239-1256, 2013.

678   Shen, Y., Fichot, C.G., and Benner, R.: Floodplain influence on dissolved organic matter

679   composition and export from the Mississippi-Atchafalaya River system to the Gulf of

680   Mexico, Limnol. Oceanogr. 57 (4), 1149-1160, 2012.

681   Testa, J.M. and Kemp, W.M.: Oxygen - Dynamics and Biogeochemical Consequences.

682   In: Wolanski, E. and McLusky, D.S. (eds.) Treatise on Estuarine and Coastal

683   Science, Vol 5, 163-199, Waltham: Academic Press, 2011.

684   Turner, R., Rabalais, N., Swenson, E., Kasprzak, M., and Romaire, T.: Summer hypoxia

685   in the Northern Gulf of Mexico and its prediction from 1978 to 1995, Mar. Environ.

686   Res., 59, 65-77, 2005.

687   Turner, R. E., Rabalais, N. N., and Justic, D.: Predicting summer hypoxia in the northern

688   Gulf of Mexico: Riverine N, P, and Si loading, Mar. Pollut. Bull., 52, 139-148, 2006.

689   Wanninkhof, R.: Relationship between wind speed and gas exchange, J. Geophys. Res.,

690   97, 7373-7382, 1992.

691   Wiseman, W., Rabalais, N., Turner, R., Dinnel, S., and MacNaughton, A.: Seasonal and

692   interannual variability within the Louisiana coastal current: stratification and

693   hypoxia, J. Mar. Syst., 12, 237-248, 1997.

Table Captions

694 **Table Captions**

695 **Table 1.** RMSE and bias (both in units of mmol O_2 m^{-3}) between simulated and observed

696 bottom DO concentrations. Comparisons were conducted over the simulation period from

697 2004 to 2007 using all available observations. Bias was calculated as model minus

698 observation. N is the number of observations available for each calculation.

699 **Table 2.** RMSE and bias (both in units of mmol O_2 m^{-2} d^{-1}) between simulated and

700 observed primary production (PP) or water column respiration (WR). Comparisons were

701 conducted over the simulation period from 2004 to 2007 using all available observations.

702 Bias was calculated as model minus observations. N is the number of observations for

703 each category.

704 **Table 3.** RMSE and bias (both in units of mmol O_2 m^{-2} d^{-1}) between simulated median of

705 sediment oxygen consumption (SOC) and observed SOC. The simulation period ranged

706 from 2004 to 2007 while observations from different sources were collected during

707 longer period from 1991 to 2011. Bias was calculated as model median minus

708 observation with same bottom dissolved oxygen (DO) concentration. N is the number of

709 observations available for each category.

710 **Table 4.** Shelf-wide average observed and simulated percentage of primary production

711 below the pycnocline (mean±standard deviation). N is the number of observations.

712 **Table 1.** RMSE and bias (both in units of mmol O_2 m^{-3}) between simulated and observed

713 bottom DO concentrations. Comparisons were conducted over the simulation period from

714 2004 to 2007 using all available observations. Bias was calculated as model minus

715 observation. N is the number of observations available for each category.

	Model		Model+CCR		
	RMSE	Bias	RMSE	Bias	N
Mississippi Delta	74.6	43.3	61.6	15.6	182
Mississippi Intermediate	72.2	40.3	61.5	18.7	845
Atchafalaya Plume	66.3	35.0	58.7	16.6	377
Mid-shelf	48.9	15.6	54.0	-18.8	435
All data	66.4	33.7	59.3	9.1	1839

716

717 **Table 2.** RMSE and bias (both in units of mmol O_2 m^{-2} d^{-1}) between simulated and

718 observed primary production (PP) or water column respiration (WR). Comparisons were

719 conducted over the simulation period from 2004 to 2007 using all available observations.

720 Bias was calculated as model minus observations. N is the number of observations for

721 each category.

	PP				WR				
	Model		Model+CCR		Model		Model+CCR		
	RMSE	Bias	RMSE	Bias	RMSE	Bias	RMSE	Bias	N
Miss. Delta	145.2	-42.3	145.5	-43.6	115.8	-49.4	104.4	-17.9	55
Miss. Inter.	94.7	10.5	95.0	9.2	93.3	-45.9	84.5	-19.4	60
Atch. Plume	114.1	12.5	114.0	11.2	62.6	-27.6	58.4	-8.2	77
Mid-shelf	91.8	50.2	91.1	48.4	75.8	-7.0	81.7	35.6	71
All data	112.0	10.8	112.0	9.3	86.5	-30.8	81.9	-1.0	263

722

723

724   **Table 3.** RMSE and bias (both in units of mmol O_2 m^{-2} d^{-1}) between simulated median of

725   sediment oxygen consumption (SOC) and observed SOC. The simulation period ranged

726   from 2004 to 2007 while observations from different sources were collected during

727   longer period from 1991 to 2011. Bias was calculated as model median minus

728   observation with same bottom dissolved oxygen (DO) concentration. N is the number of

729   observations available for each category.

	Model		Model+CCR		
	RMSE	Bias	RMSE	Bias	N
Rowe et al. 2012	15.9	11.1	13.6	8.0	12
McCarthy et al. 2013	15.8	10.2	13.9	7.0	18
Lehrter et al. 2012	26.1	24.6	22.4	20.7	22
Murrell and Lehrter 2011	24.7	21.2	21.7	18.1	31
All data	22.3	18.2	19.5	14.9	83

730

731   **Table 4.** Shelf-wide average observed and simulated percentage of primary production

732   below the pycnocline (mean±standard deviation). N is the number of observations.

Cruise	N	Percentage of PP below pycnocline (%)	
		Observation	Simulation
Mar 2005	24	23.3±29.4	27.8±26.9
Apr 2006	31	35.3±30.0	23.4±25.2
Jun 2006	54	29.3±25.7	18.6±19.2
Sep 2006	71	38.7±25.7	39.4±28.2
May 2007	64	25.8±25.0	36.2±29.6
Aug 2007	60	24.7±23.3	40.9±30.9
RMSE			42.5
Bias			2.8
N			304

733 **Figure Captions**

734 **Fig. 1.** Model grid (light grey lines) and bathymetry (in meters). The black lines delineate

735 areas used during model analysis and are referred to as Mississippi Delta, Mississippi

736 Intermediate, Atchafalaya Plume and Mid-shelf region in the text. The black dots are

737 stations where primary production (Lehrter et al. 2009) and respiration rates (Murrell et

738 al. 2013) were collected.

739 **Fig. 2.** Mississippi and Atchafalaya River freshwater discharge (upper panel) and nutrient

740 loads (lower panel) in 2004-2007. The dash line indicates the long-term climatology

741 (1983-2010).

742 **Fig. 3.** Schematic of the biological model.

743 **Fig. 4.** Time series of simulated and observed dissolved oxygen concentration (DO) in

744 bottom water in the Mississippi Delta, Mississippi Intermediate, Atchafalaya Plume and

745 Mid-shelf regions. For the simulations, the medians are shown as solid lines (Model:

746 blue line, Model+CCR: red line), the range between the 25th and 75th percentiles as dark

747 blue/red area and the range between the minimum and maximum value as light blue/red

748 area. For the observations, the medians of monthly binned observations are shown as

749 black dots, the range between the 25th and 75th percentiles as thick vertical lines and the

750 range between minimum and maximum values as thin vertical lines. The number of

751 observations in each monthly bin is given above each maximum value. The dashed line

752 indicates the hypoxia criterion of 62.5 mmol O_2 m^{-3}. Observations are from Rabalais et al.

753 (2007), Lehrter et al. (2009, 2012), Nunnally et al. (2012), Murrell et al. (2014), and the

754 MCH program.

755 **Fig. 5.** Vertical profiles of model bias (model minus observations, mmol O_2 m^{-3}) in

756 dissolved oxygen (DO) calculated from 2004 to 2007 for June to August in the 4 sub-

757 regions. The vertical axis is the scaled depth, where 0 corresponds to the surface and -1 to

758 the bottom. The light grey areas represent the standard deviation in the observations.

759 Observations are from Rabalais et al. (2007), Lehrter et al. (2009, 2012), Murrell et al.

760 (2014), and the MCH program.

761 **Fig. 6.** Vertically integrated rates of observed and simulated primary production (upper

762 panel) and water column respiration (lower panel) in the 4 sub-regions. The error bars

763 indicate the standard deviation. The number of observations in each sub-region is given

764 above the error bars.

765 **Fig. 7.** Model simulated sediment oxygen consumption (SOC) versus bottom dissolved

766 oxygen (DO) for the period 2004 to 2007, including the median (solid line) and the range

767 between 25th and 75th percentiles (shaded area). Also shown for comparison are

768 observations from Rowe et al. (2002), McCarthy (2013), Lehrter et al. (2012) and Murrell

769 and Lehrter (2011).

770 **Fig. 8.** Simulated net community production (PP-TR) versus air-sea flux of oxygen for

771 the 4 sub-regions. The colored dots represent monthly means averaged over 2004 to

772 2007. Positive air-sea flux indicates oxygen is taken by water whereas negative air-sea

773 flux indicates oxygen outgasses. Positive (PP-TR) suggests autotrophic whereas negative

774 (PP-TR) suggests heterotrophic. Standard deviations of the air-sea flux in different

775 months and sub-regions range widely from 13 to 58 mmol O_2 m^{-2} d^{-1} and standard

776 deviation of (PP-TR) range from 12 to 63 mmol O_2 m^{-2} d^{-1}, both of which are higher in

777 Mississippi Delta and Atchafalaya Plume and lower in the other two regions.

778 **Fig. 9.** Simulated 4-year (2004-2007) mean oxygen balance in summer for the 4 sub-

779 regions. Oxygen source and sink terms are given for the surface layer above the

780 pycnocline, for the mid layer and for the 5-m thick bottom layer. The average depth of

781 the pycnocline, depth at 5 m above bottom and the average water column depth are

782 indicated for each sub-region. The open circles indicate the balance of primary

783 production (PP) and respiration+nitrification (WR) in each layer. For the bottom layer,

784 the bars for respiration+nitrification (WR) and sediment oxygen consumption (SOC) are

785 shown stacked and SOC is repeated separately. The net rate of oxygen change in each

786 layer (i.e. the sum of all oxygen source and sink terms) is given and denoted as Net.

787 **Fig. 10.** Time series of simulated hypoxic extent for the full model (black line) and the

788 model without biological processes in the water column (red line). Also shown is the

789 observed hypoxic extent in late July (black dots). The observed hypoxic extent was

790 estimated by linearly interpolating the observed oxygen concentrations onto the model

791 grid and then calculating the area with oxygen concentrations below the hypoxic

792 threshold (Fennel et al., 2013).

793

794
795 **Fig. 1.** Model grid (light grey lines) and bathymetry (in meters). The black lines delineate

796 areas used during model analysis and are referred to as Mississippi Delta, Mississippi

797 Intermediate, Atchafalaya Plume and Mid-shelf region in the text. The black dots are

798 stations where primary production (Lehrter et al. 2009) and respiration rates (Murrell et
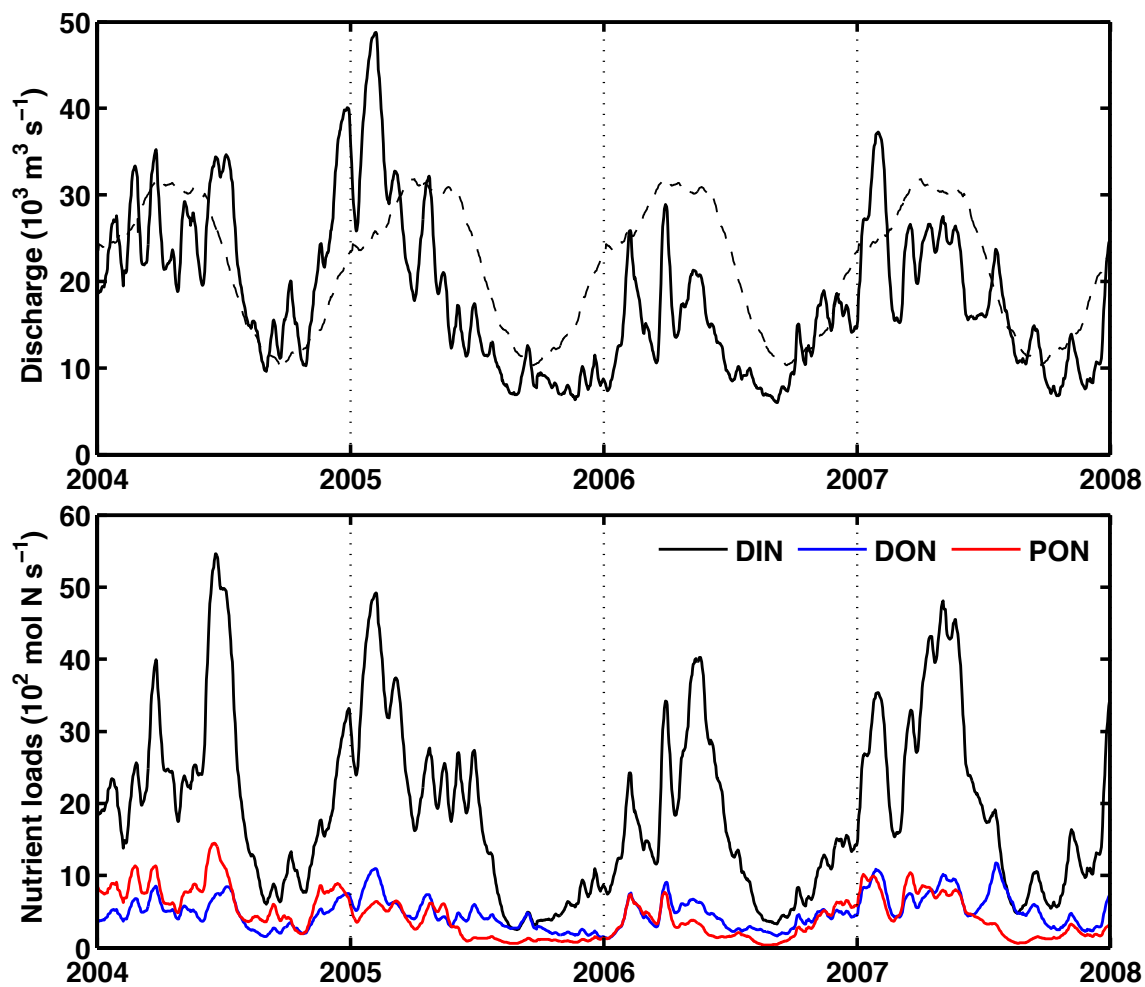
799 al. 2013) were collected.

800

Fig. 2. Mississippi and Atchafalaya River freshwater discharge (upper panel) and nutrient
loads (lower panel) in 2004-2007. The dash line indicates the long-term climatology
(1983-2010).

804
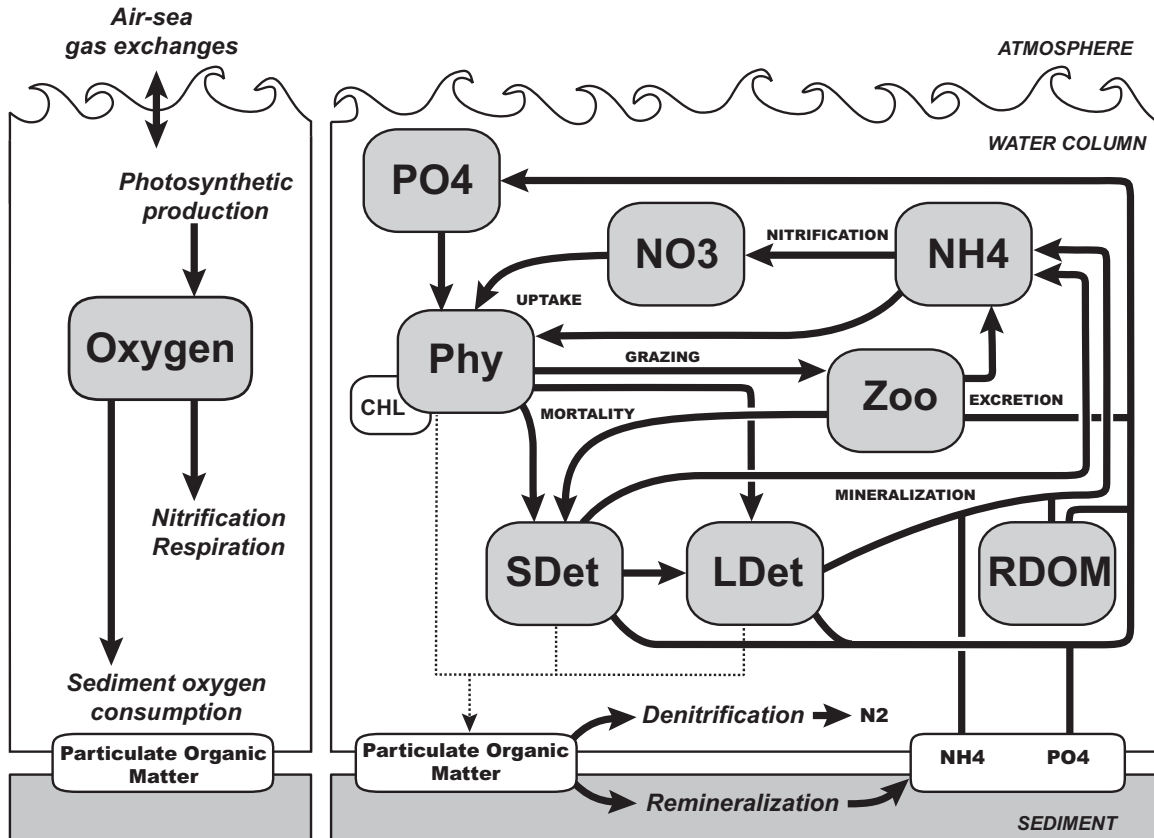
Fig. 3. Schematic of the biological model.
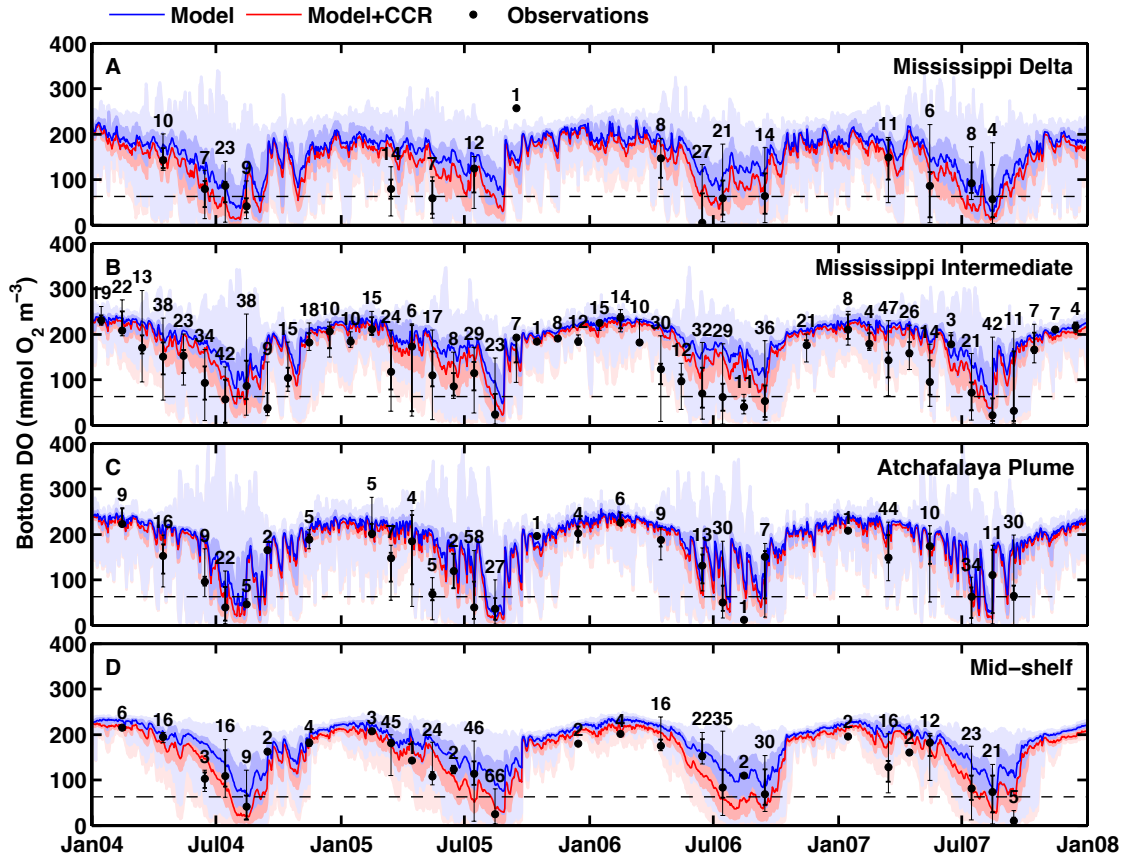
Fig. 4. Time series of simulated and observed dissolved oxygen concentration (DO) in bottom water in the Mississippi Delta, Mississippi Intermediate, Atchafalaya Plume and Mid-shelf regions. For the simulations, the medians are shown as solid lines (Model: blue line, Model+CCR: red line), the range between the 25th and 75th percentiles as dark blue/red area and the range between the minimum and maximum value as light blue/red area. For the observations, the medians of monthly binned observations are shown as black dots, the range between the 25th and 75th percentiles as thick vertical lines and the range between minimum and maximum values as thin vertical lines. The number of observations in each monthly bin is given above each maximum value. The dashed line indicates the hypoxia criterion of 62.5 mmol O_2 m^{-3}. Observations are from Rabalais et al.

42

817   (2007), Lehrter et al. (2009, 2012), Nunnally et al. (2012), Murrell et al. (2013b), and the

818   MCH program.

819
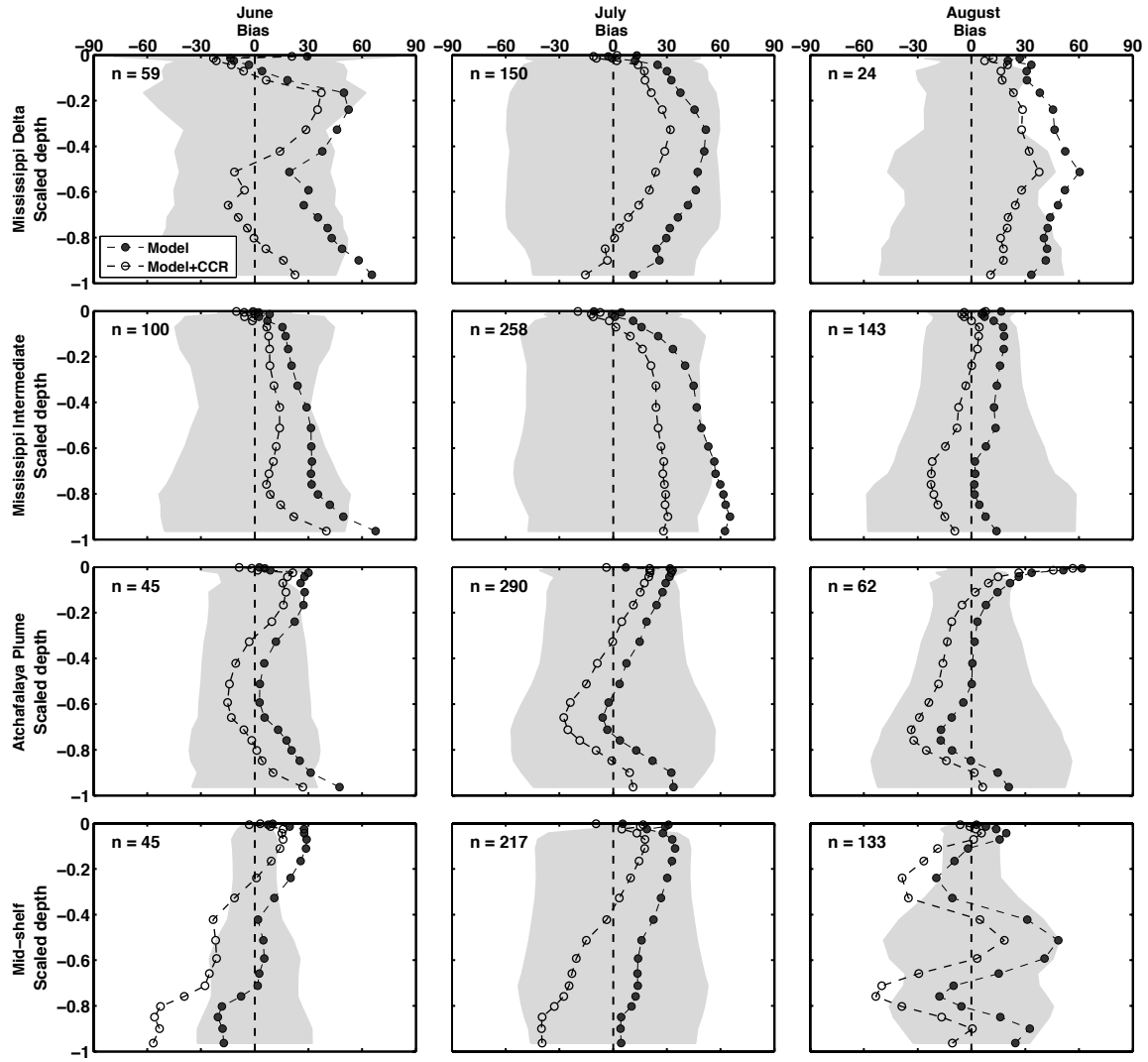
820   **Fig. 5.** Vertical profiles of model bias (model minus observations, mmol O_2 m^{-3}) in

821   dissolved oxygen (DO) calculated from 2004 to 2007 for June to August in the 4 sub-

822   regions. The vertical axis is the scaled depth, where 0 corresponds to the surface and -1 to

823   the bottom. The light grey areas represent the standard deviation in the observations.

824   Observations are from Rabalais et al. (2007), Lehrter et al. (2009, 2012), Murrell et al.

825   (2013b), and the MCH program.

826
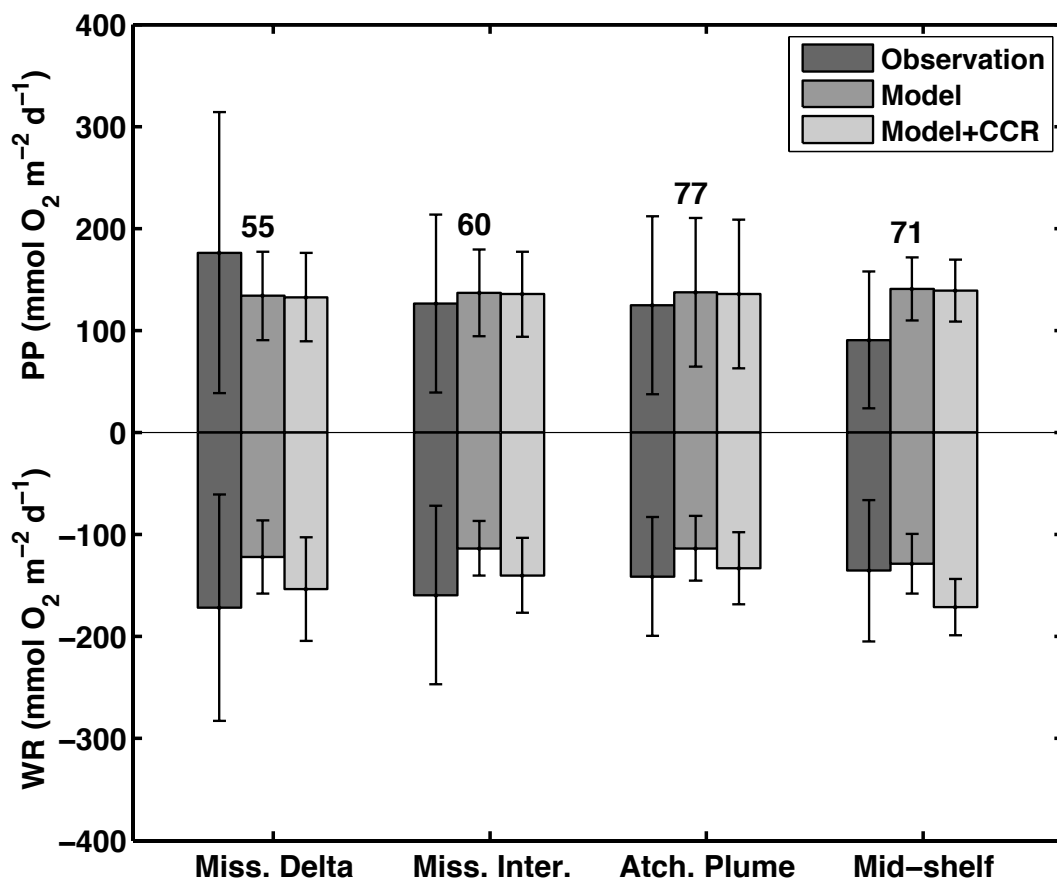
Fig. 6. Vertically integrated rates of observed and simulated primary production (upper panel) and water column respiration (lower panel) in the 4 sub-regions. The error bars indicate the standard deviation. The number of observations in each sub-region is given above the error bars.
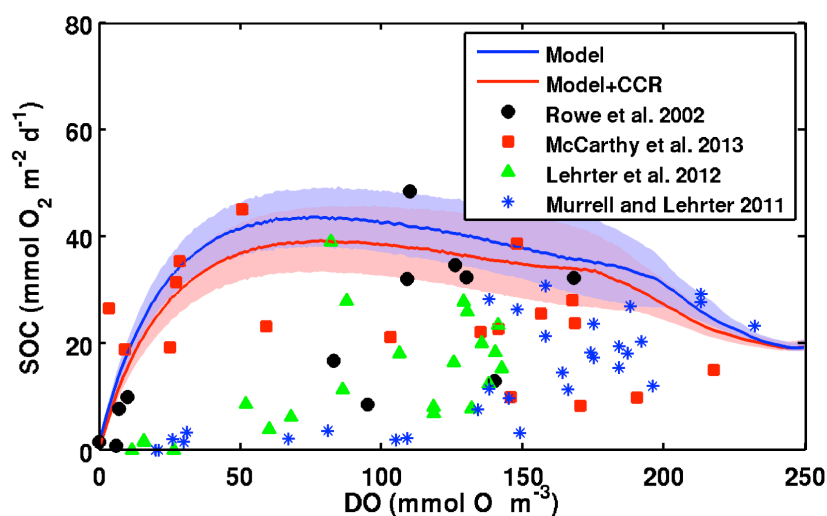
832

Fig. 7. Model simulated sediment oxygen consumption (SOC) versus bottom dissolved oxygen (DO) for the period 2004 to 2007, including the median (solid line) and the range between 25th and 75th percentiles (shaded area). Also shown for comparison are observations from Rowe et al. (2002), McCarthy (2013), Lehrter et al. (2012) and Murrell and Lehrter (2011).
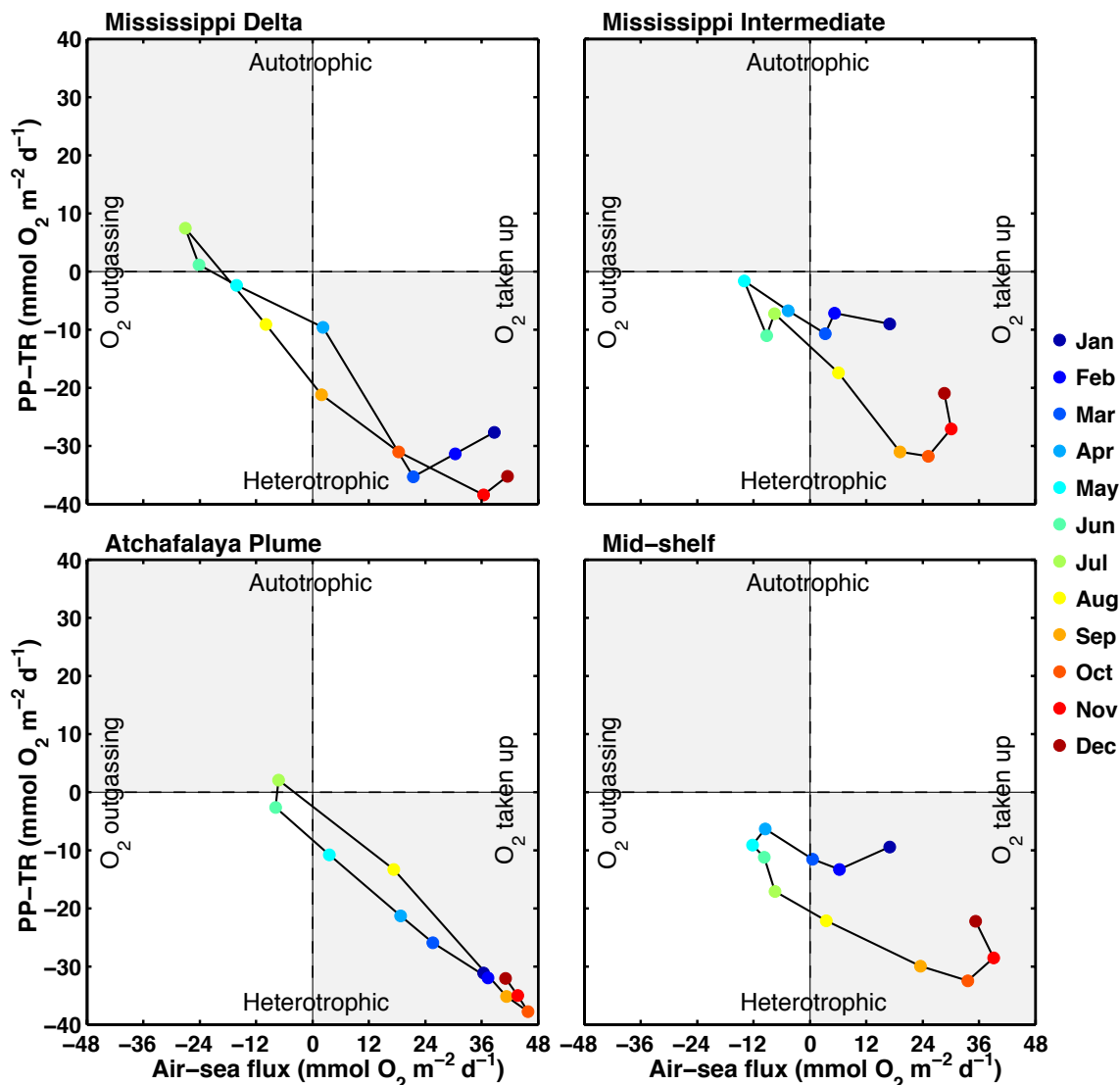
838

Fig. 8. Simulated net community production (PP-TR) versus air-sea flux of oxygen for
the 4 sub-regions. The colored dots represent monthly means averaged over 2004 to
2007. Positive air-sea flux indicates oxygen is taken by water whereas negative air-sea
flux indicates oxygen outgasses. Positive (PP-TR) suggests autotrophic whereas negative
(PP-TR) suggests heterotrophic. Standard deviations of the air-sea flux in different
months and sub-regions range widely from 13 to 58 mmol O_2 m^{-2} d^{-1} and standard
deviation of (PP-TR) range from 12 to 63 mmol O_2 m^{-2} d^{-1}, both of which are higher in
Mississippi Delta and Atchafalaya Plume and lower in the other two regions.
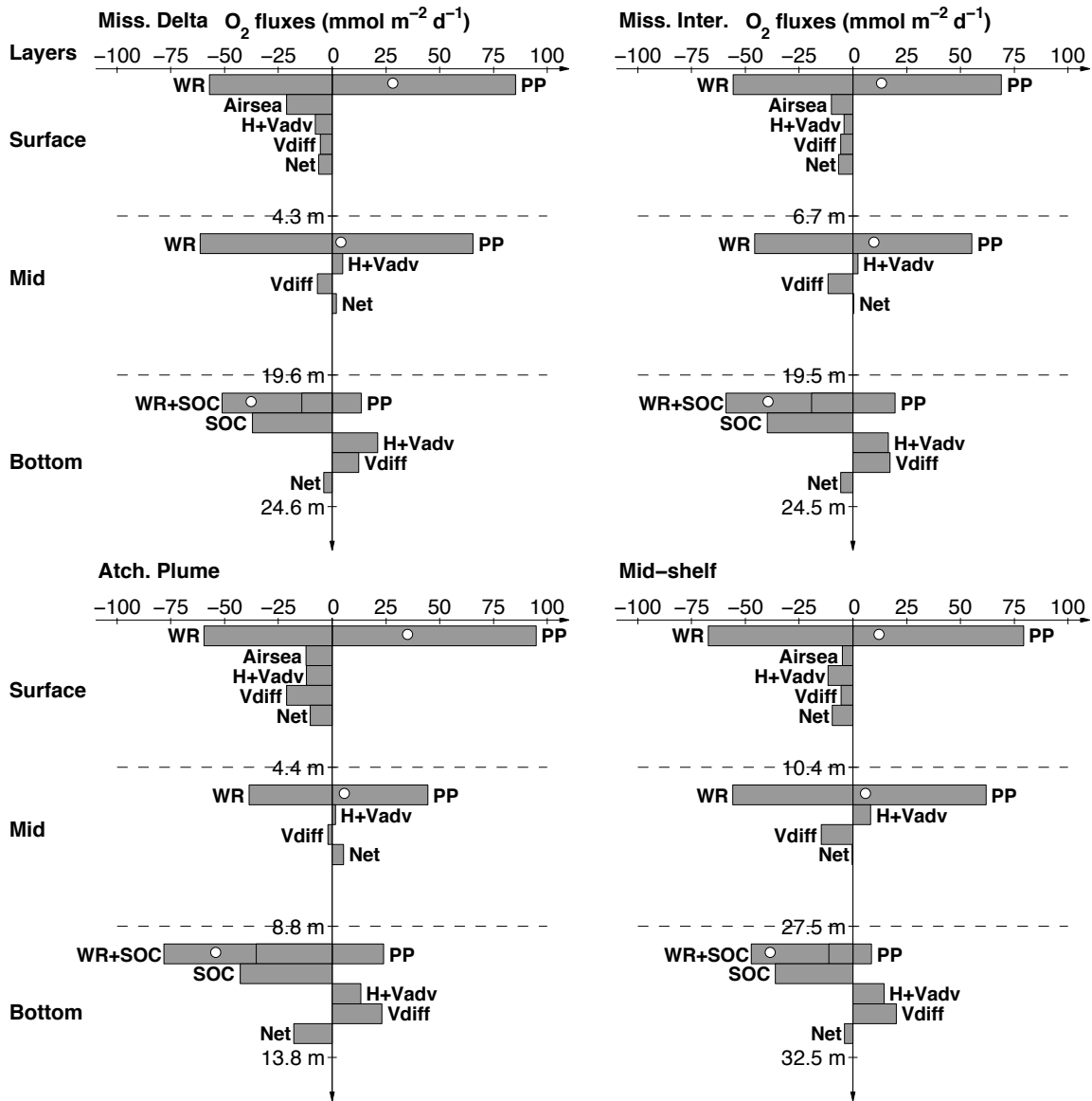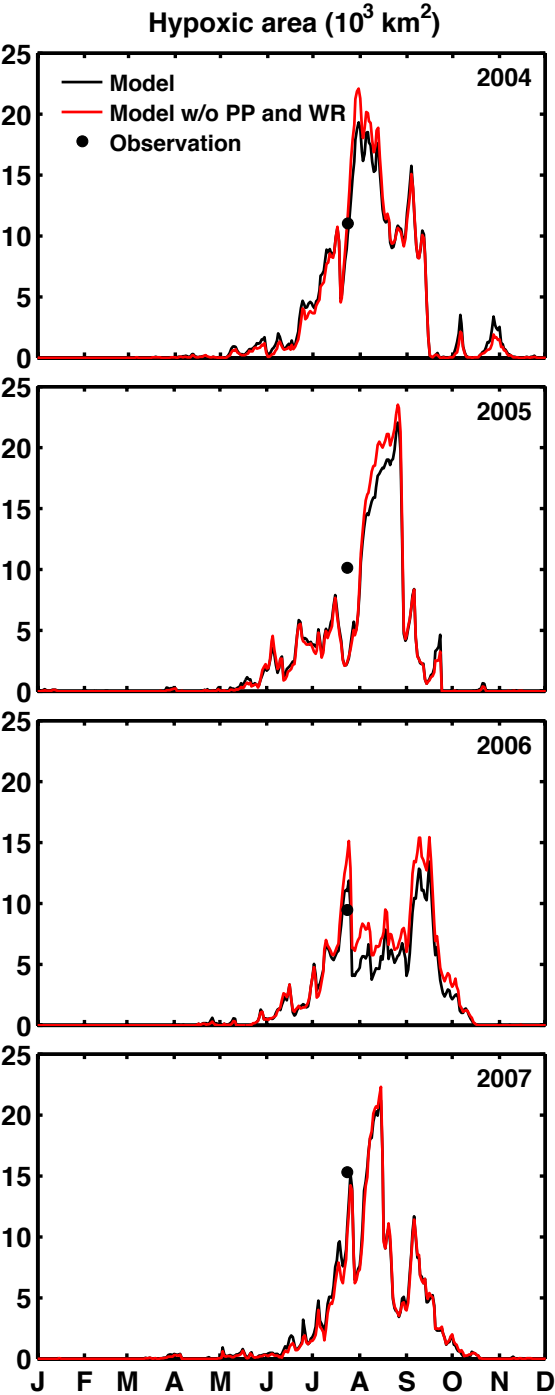
847

Fig. 9. Simulated 4-year (2004-2007) mean oxygen balance in summer for the 4 sub-regions. Oxygen source and sink terms are given for the surface layer above the pycnocline, for the mid layer and for the 5-m thick bottom layer. The average depth of the pycnocline, depth at 5 m above bottom and the average water column depth are indicated for each sub-region. The open circles indicate the balance of primary production (PP) and respiration+nitrification (WR) in each layer. For the bottom layer, the bars for respiration+nitrification (WR) and sediment oxygen consumption (SOC) are

855 shown stacked and SOC is repeated separately. The net rate of oxygen change in each

856 layer (i.e. the sum of all oxygen source and sink terms) is given and denoted as Net.

857

Hypoxic area (10^3 km^2)

858

859 **Fig. 10.** Time series of simulated hypoxic extent for the full model (black line) and the

860 model without biological processes in the water column (red line). Also shown is the

861 observed hypoxic extent in late July (black dots). The observed hypoxic extent was

862 estimated by linearly interpolating the observed oxygen concentrations onto the model

863 grid and then calculating the area with oxygen concentrations below the hypoxic

864 threshold (Fennel et al., 2013).